Electronic Supplementary Information for

Polyoxometalate-based Yolk@Shell Dual Z-scheme Superstructure Tandem Heterojunction Nanoreactors: Encapsulation and Confinement Effects

Chunxu Wu[a], Zipeng Xing[a,*], Bin Fang[a], Yongqian Cui[a], Zhenzi Li[b,*], Wei Zhou[a,b,*]

[a] Department of Environmental Science, School of Chemistry and Materials Science, Key Laboratory of Functional Inorganic Material Chemistry, Ministry of Education of the People's Republic of China, Heilongjiang University, Harbin 150080, P. R. China,

Tel: +86-451-8660-8616, Fax: +86-451-8660-8240,

Email: xingzipeng@hlju.edu.cn; zwchem@hotmail.com

[b] Shandong Provincial Key Laboratory of Molecular Engineering, School of Chemistry and Chemical Engineering, Qilu University of Technology (Shandong Academy of Sciences), Jinan 250353, P. R. China

Email: zhenzhenlee2014@163.com

Experimental section

1. Materials

Phosphotungstic acid hydrate ($H_3PW_{12}O_{40}\cdot xH_2O$) and Indium chloride tetrahydrate ($InCl_3\cdot 4H_2O$) were purchased from Shanghai Aladdin Biochemical Technology Co., Ltd. Potassium chloride (KCl) was purchased from Tianjin Aopusheng Chemical Co., Ltd. Zinc chloride ($ZnCl_2$) and Thioacetamide (TAA) were purchased from Shanghai Macklin Biochemical Co., Ltd. Silver nitrate ($AgNO_3$) and absolute ethanol (EtOH) were purchased from Tianjin Kermel Chemical Reagent Co., Ltd. Sodium sulfide nonahydrate ($Na_2S\cdot 9H_2O$) was purchased from Tianjin Hengxing Chemical Reagent Co., LTD. All of the reagents which were used in the experiments were analytical grade and employed without further purification, and the deionized water was used throughout the study.

2. Characterization

The microcrystalline structure, surface characteristics and element distribution of these samples were examined by Scanning electron microscopy (SEM, Hitachi S-4800) with energy-dispersive X-ray spectrometer (EDX) operated at an accelerating voltage of 20 kV. Transmission electron microscopy (TEM) and high-resolution transmission (HRTEM) images were obtained by (JEM-2100 TEM) electron microscope. The as-synthesized samples were confirmed by powder X-ray diffraction (XRD) on a Bruker D8 advance under Cu Kα (λ = 1.5406 Å) radiation and the result was collected. X-ray photoelectron spectroscopy (XPS) was measured on a PHI-5700 ESCA instrument with Al-Kα X-ray source. Specific surface areas were characterized

by Brunauer-Emmett-Teller (BET) at liquid nitrogen temperature, using AUTOSORB-1 instrument. The optical diffuse reflectance spectrum was conducted on a UV-vis-NIR scanning spectrophotometer (UV3600, Shimadzu) using an integrating sphere accessory. The •OH were detected by the fluorescence probe technique with coumarin on a RF-5301PC fluorescence spectrophotometer and a 300 W xenon lamp with UVIRCUT filter (420-780 nm) was used as visible-light source. Electron spin response (ESR) spectra was recorded on an ER200-SRC spectrometer under visible-light illumination. The PL spectra were recorded on a fluorescence spectrophotometer (Fluorolog-Tau-3, America), excited at 325 nm. The work function was tested by Scanning Kelvin probe (SKP) (SKP5050 system, Scotland).

3. Photocatalytic degradation activity test

Tetracycline hydrochloride was selected to test the photocatalytic degradation performance. The experiment was carried out in the winter in Harbin (44° 04′ N and 125° 42′ E), and the room temperature was kept at 12 ± 2 °C. In a typical experiment, the photocatalysts (8 mg) was added to tetracycline hydrochloride solution (40 mL, 20 mg L^{-1}). Then, the suspension was placed in the dark to ensure adsorption-desorption equilibrium. The suspension was irradiated with a 300 W Xenon lamp equipped with UVCUT filter ($\lambda \geq 420$ nm). The residual tetracycline hydrochloride concentrations were analyzed by T6 UV-vis spectrophotometer.

4. Photocatalytic hydrogen evolution

Photocatalytic H_2 evolution experiment was carried out in a photocatalytic hydrogen production system (AuLight, Beijing, CEL-SPH2N). In the photocatalytic hydrogen

evolution reaction, mixing aqueous solution of the photocatalyst (50 mg) with 10 vol% triethanolamine solution which is used as a sacrificial agent. Before visible light exposure, the reactor and the entire gas circulation system are completely degassed by vacuum pump to remove air for 30 min. The 300 W Xenon is then fitted with optical filter ($\lambda \geq 420$ nm) as a visible light source. The evolution of photocatalytic H_2 was analyzed by gas chromatograph (SP7800, TCD, molecular sieve 5a, N_2 carrier, Beijing Keruida Limited.).

5. Photoelectrochemical measurement

The electrochemical impedance spectroscopy and photocurrents curves were examined by the Princeton workstation, which employed the three-electrode configuration. Na_2SO_4 (0.1 M) aqueous solution was used as the electrolyte solution. Pt foil was the counter electrode and Ag/AgCl electrode was used as the reference electrode. In order to prepare working electrode, photocatalyst sample (50 mg) was dispersed in ethanol (35 mL), and then the suspension was sprayed onto the FTO glass, and then the FTO glass was calcined at 200 °C for 2 h in Ar. Furthermore, a 300 W Xenon lamp with UVIRCUT filter (420-780 nm) was used as visible-light source. Electro-chemical impedance spectroscopy was measured with amplitude of 5 mV and frequencies varying from 0.01 to 10000 Hz.

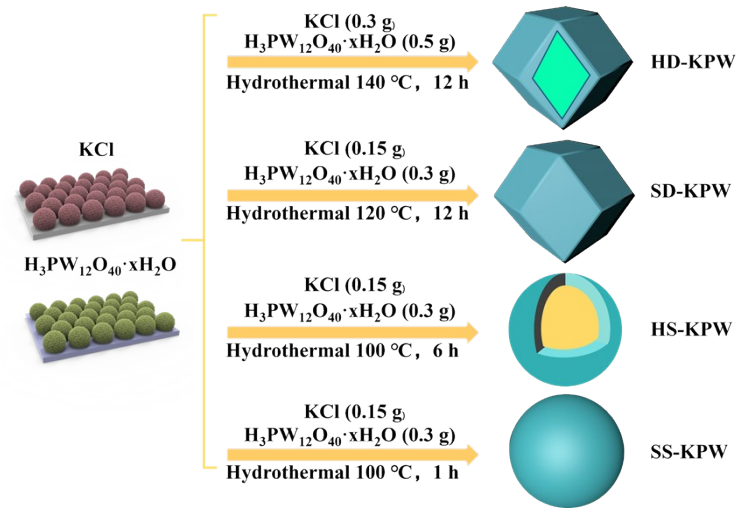

Fig. S1. Schematic illustration of the synthesis of HD-KPW, SD-KPW, HS-KPW and SS-KPW.

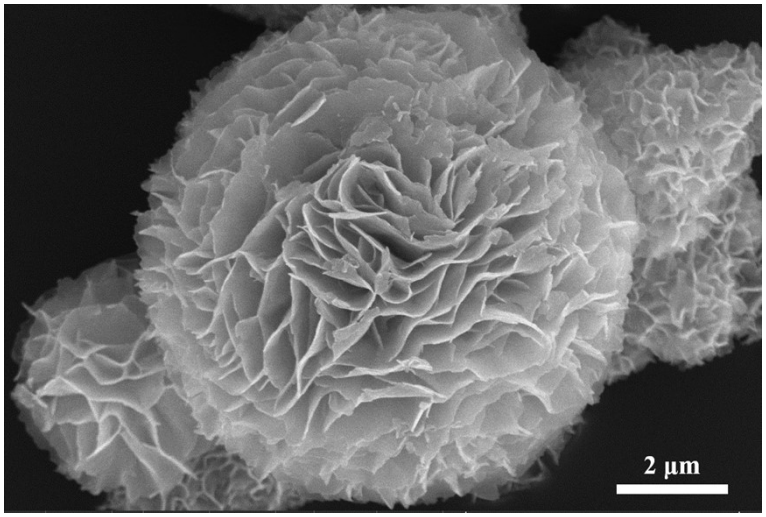

Fig. S2. The SEM image of the individually grown ZIS.

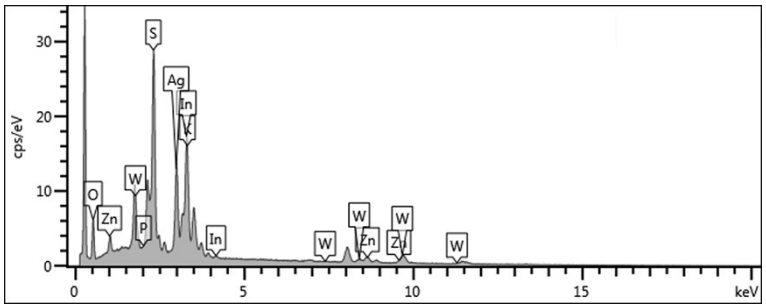

Fig. S3. The EDX elemental spectrum of ZIS@HD-KPW@ZIS/AS.

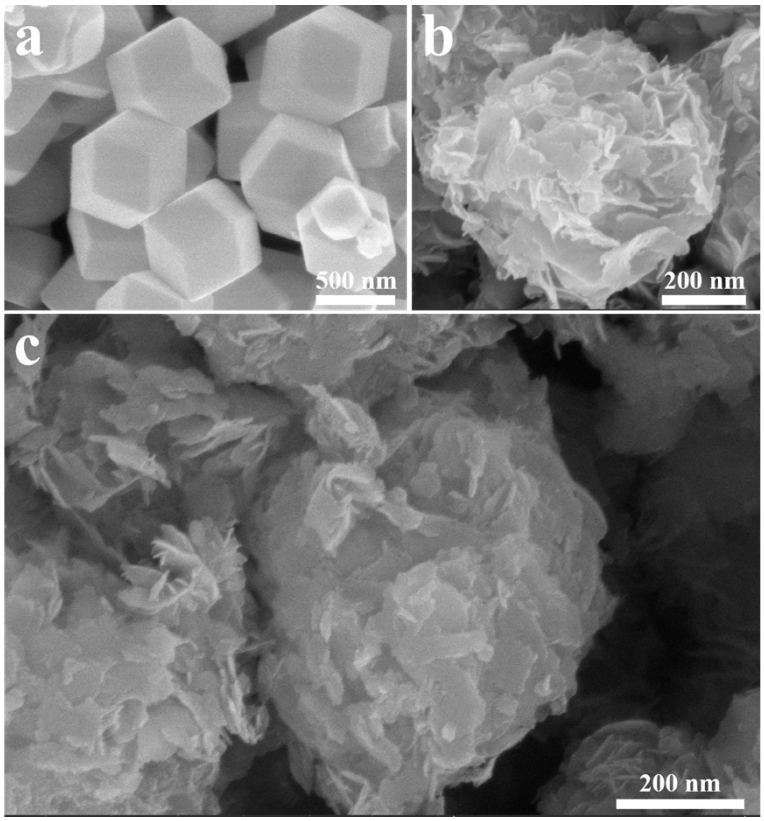

Fig. S4. The SEM images of SD-KPW (a), SD-KPW@ZIS (b) and SD-KPW@ZIS/AS (c).

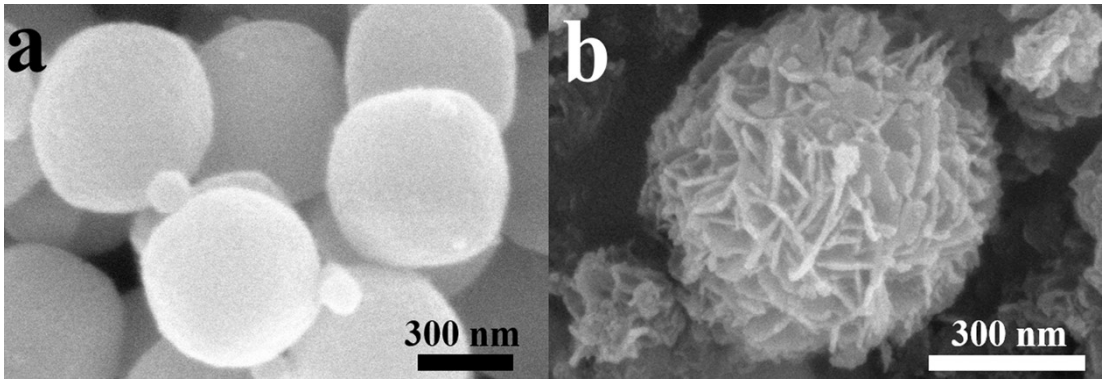

Fig. S5. The SEM images of HS-KPW (a) and ZIS@HS-KPW@ZIS/AS (b).

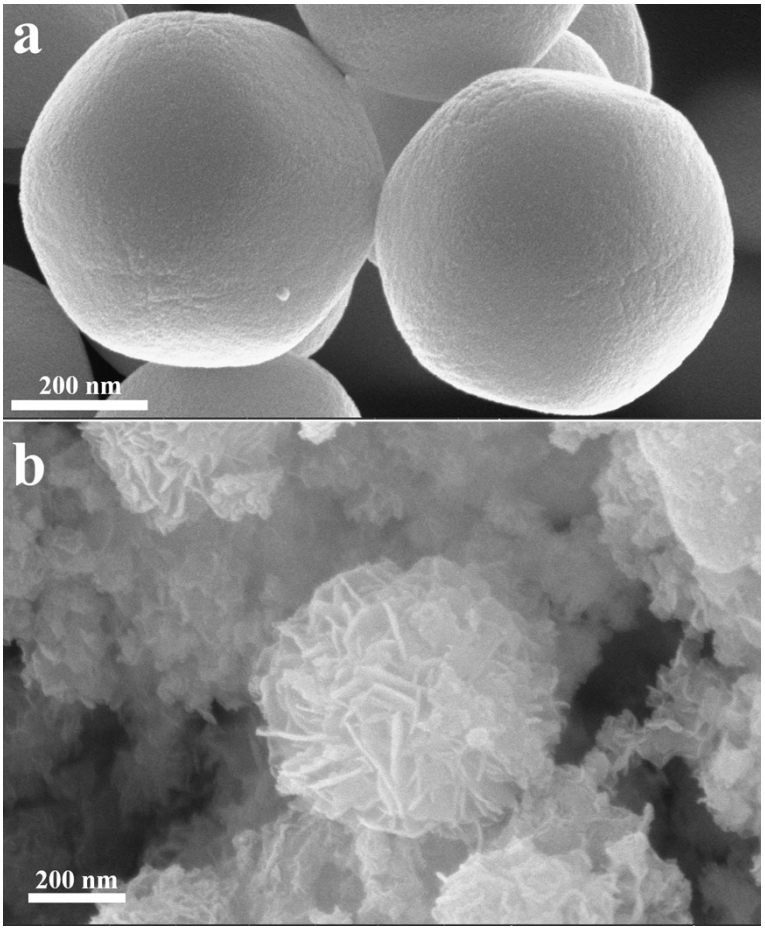

Fig. S6. The SEM images of SS-KPW (a) SS-KPW@ZIS/AS (b).

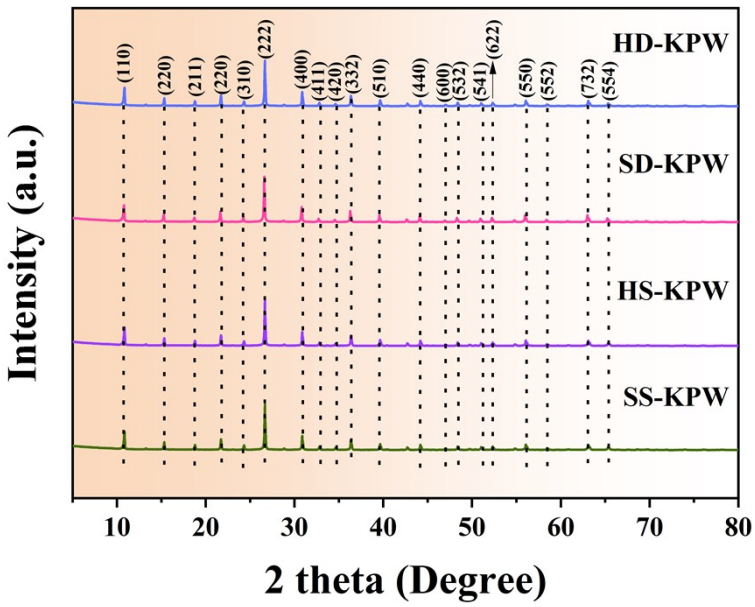

Fig. S7. Typical XRD patterns of HD-KPW, SD-KPW, HS-KPW and SS-KPW.

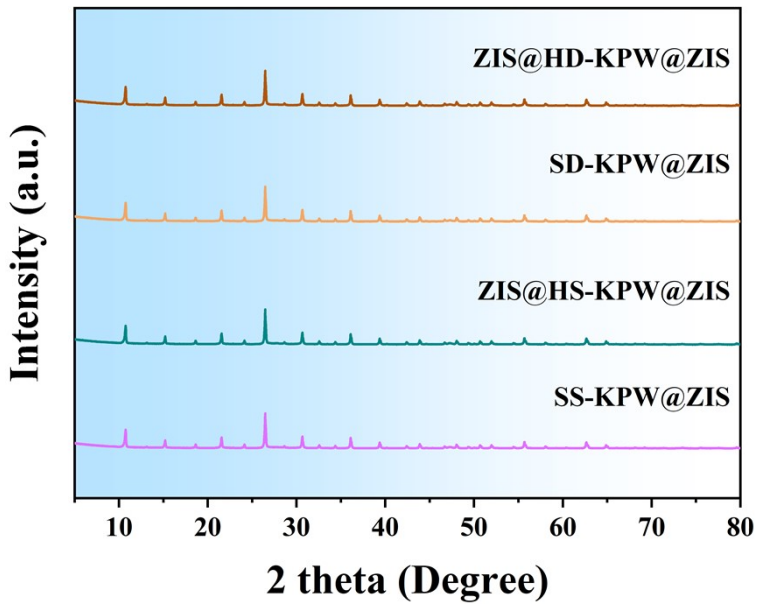

Fig. S8. Typical XRD patterns of ZIS@HD-KPW@ZIS, SD-KPW@ZIS, ZIS@HS-KPW@ZIS and SS-KPW@ZIS.

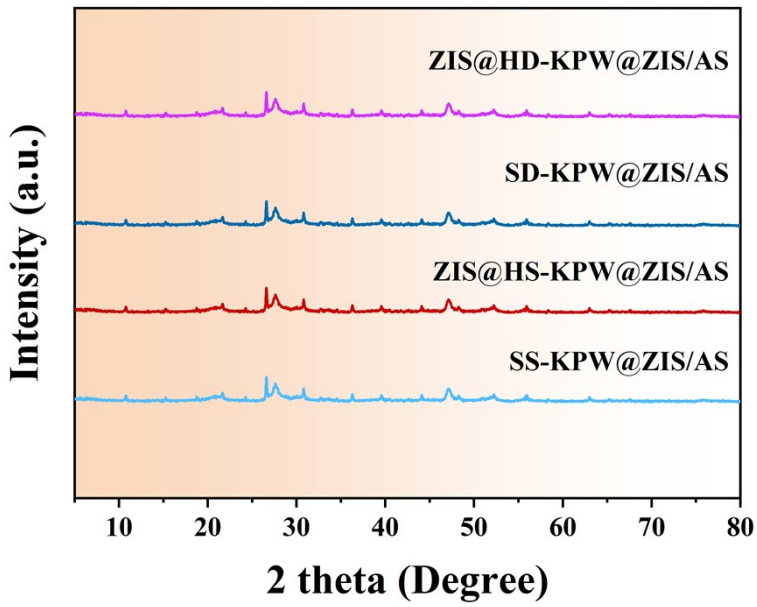

Fig. S9. Typical XRD patterns of ZIS@HD-KPW@ZIS/AS, SD-KPW@ZIS/AS, ZIS@HS-KPW@ZIS/AS and SS-KPW@ZIS/AS.

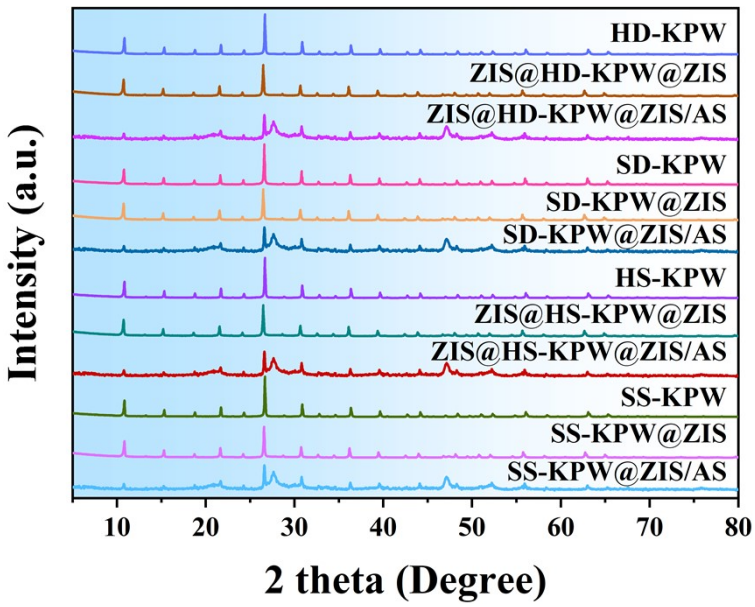

Fig. S10. Typical XRD patterns of twelve as-prepared samples.

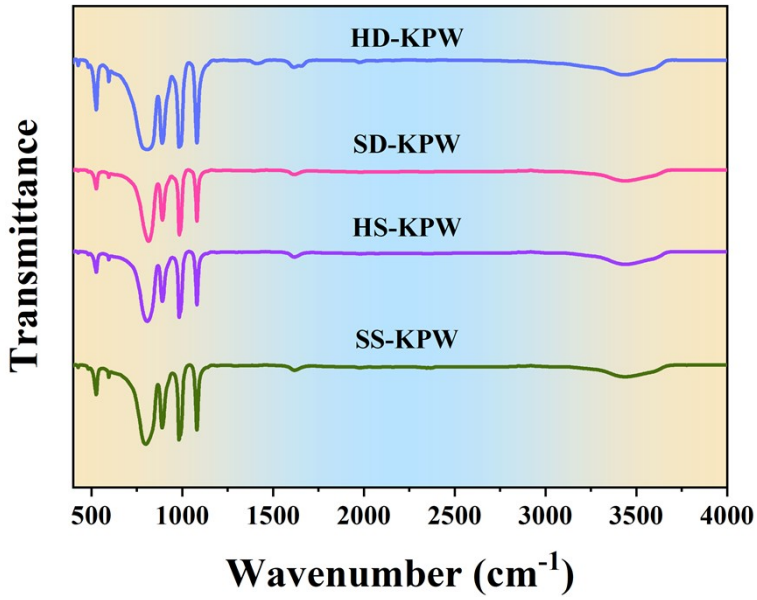

Fig. S11. The FT-IR spectra of HD-KPW, SD-KPW, HS-KPW and SS-KPW.

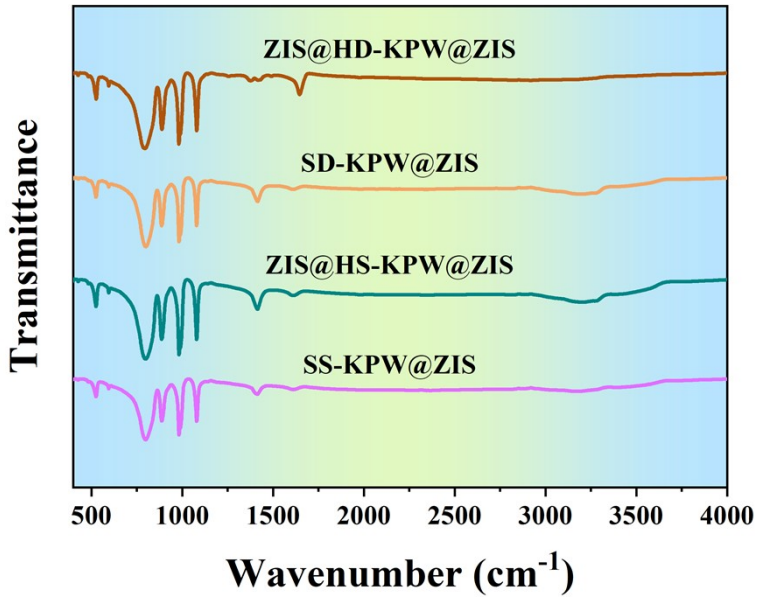

Fig. S12. The FT-IR spectra of ZIS@HD-KPW@ZIS, SD-KPW@ZIS, ZIS@HS-KPW@ZIS and SS-KPW@ZIS.

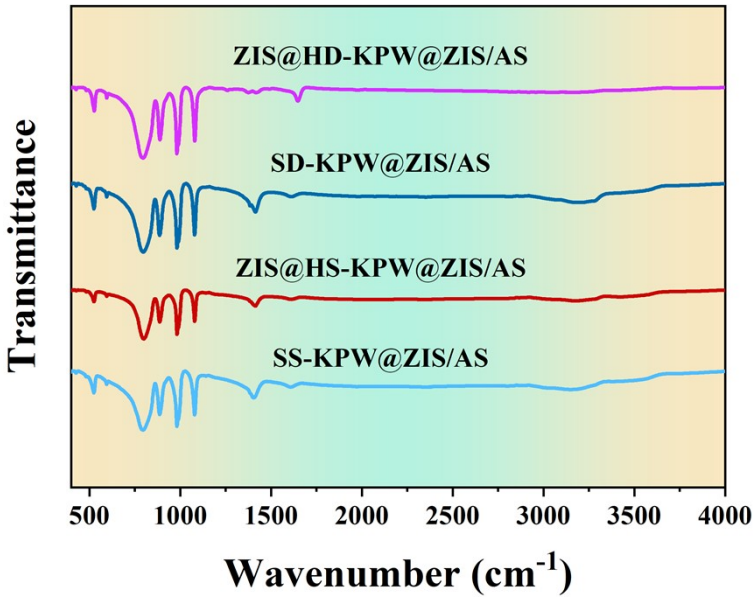

Fig. S13. The FT-IR spectra of ZIS@HD-KPW@ZIS/AS, SD-KPW@ZIS/AS, ZIS@HS-KPW@ZIS/AS and SS-KPW@ZIS/AS.

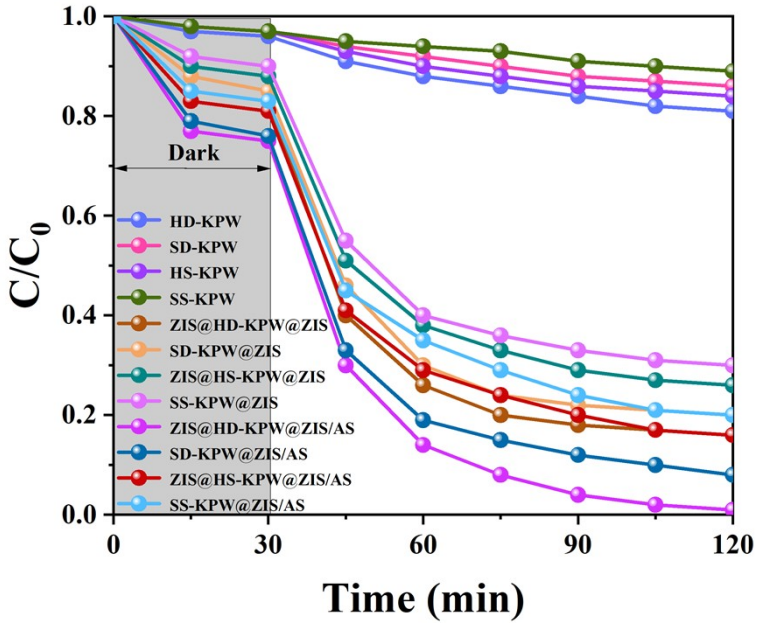

Fig. S14. The photocatalytic degradation curves of tetracycline hydrochloride for twelve as-prepared samples.

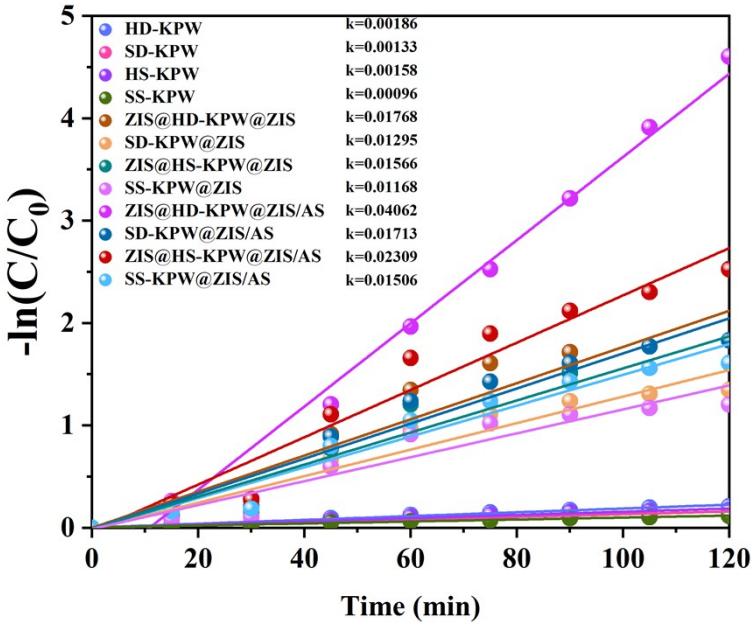

Fig. S15. The photocatalytic degradation plots of twelve as-prepared samples with the apparent reaction rate constants k for the degradation of tetracycline hydrochloride.

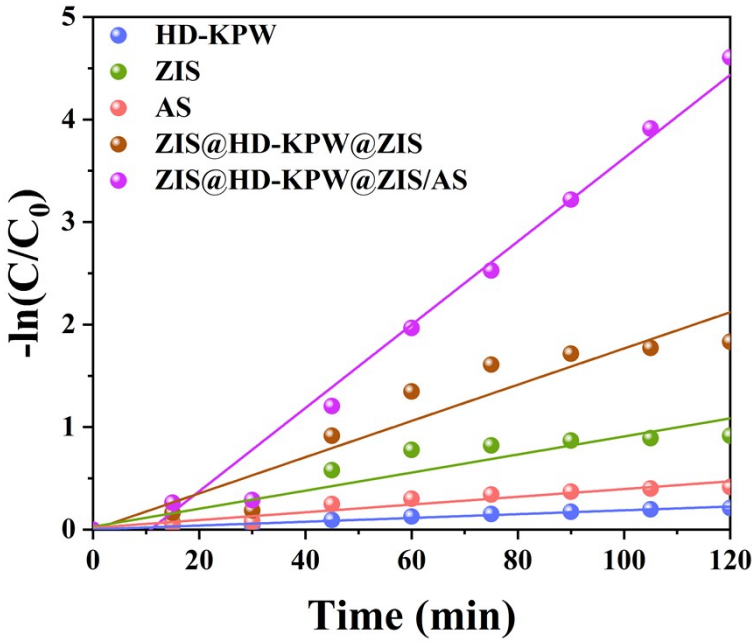

Fig. S16. The photocatalytic degradation plots of five selected samples with the apparent reaction rate constants k for the degradation of tetracycline hydrochloride.

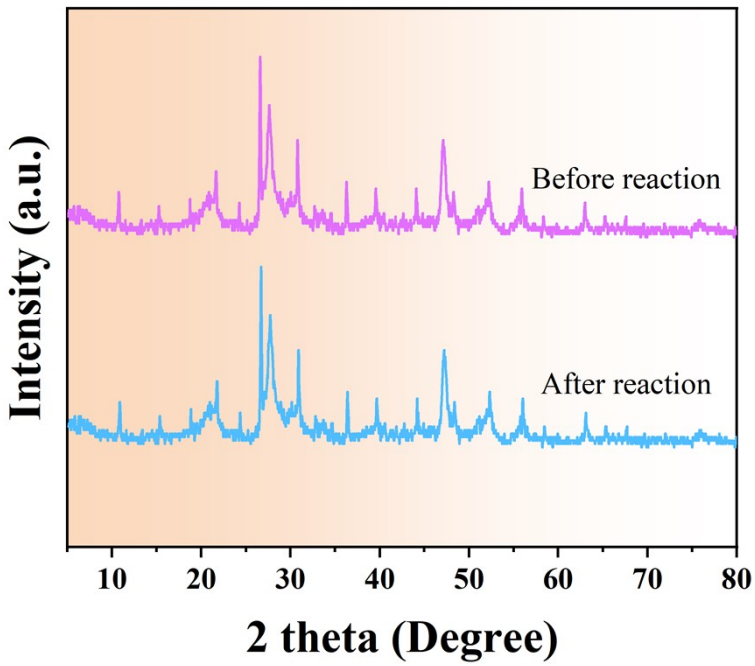

Fig. S17. XRD patterns of ZIS@HD-KPW@ZIS/AS before and after ten cycles photocatalytic degradation for tetracycline hydrochloride under visible light irradiation.

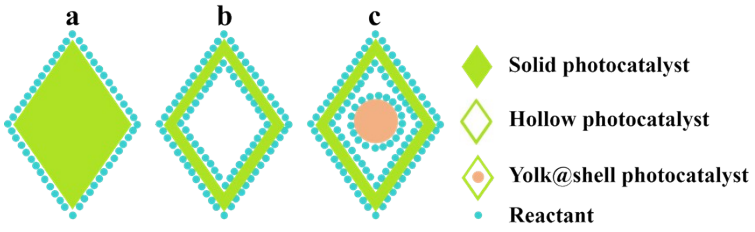

Fig. S18. The schematic diagram of reactants adsorption on the surface of solid (a), hollow (b) and yolk@shell photocatalyst (c).

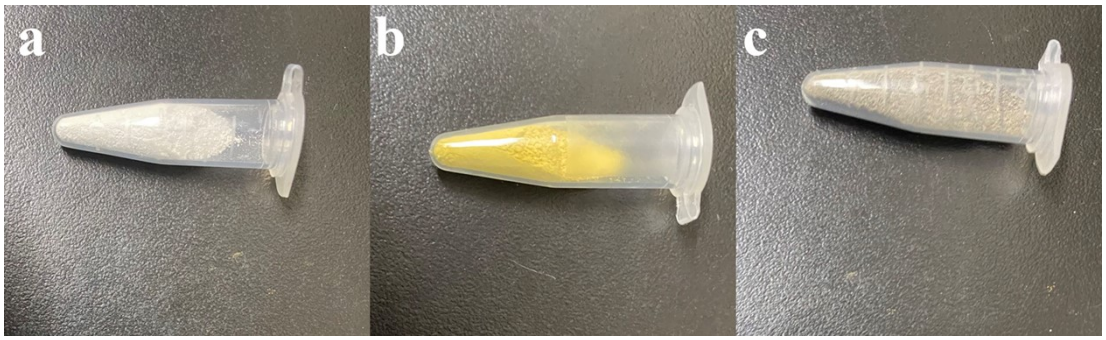

Fig. S19. The digital photos of white HD-KPW (a), yellow ZIS@HD-KPW@ZIS (b), and brown-black ZIS@HD-KPW@ZIS/AS (c).

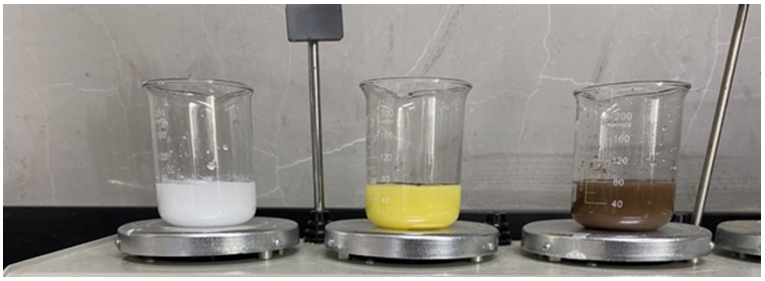

Fig. S20. The digital photos of the as-prepared photocatalysts which were dispersed in water and then placed on a magnetic stirrer for stirring: from left to right were white HD-KPW, yellow ZIS@HD-KPW@ZIS, and brown-black ZIS@HD-KPW@ZIS/AS, respectively.

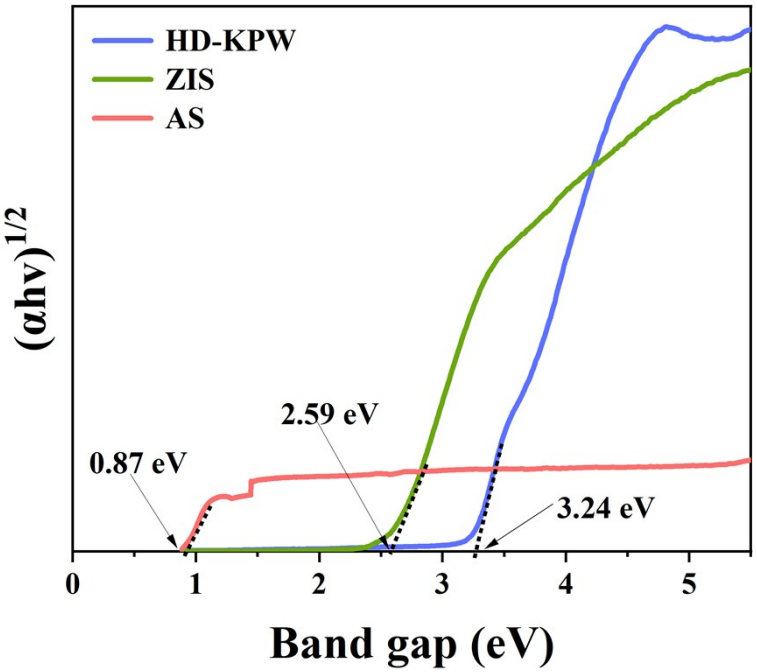

Fig. S21. Typical Tauc plots for indirect band gaps of HD-KPW, ZIS and AS.

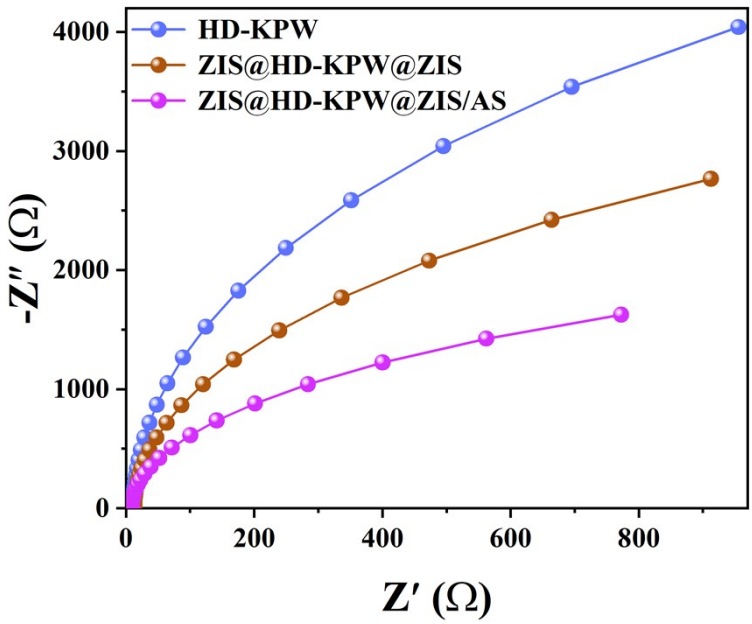

Fig. S22. EIS Nyquist plots of HD-KPW, ZIS@HD-KPW@ZIS and ZIS@HD-KPW@ZIS/AS.

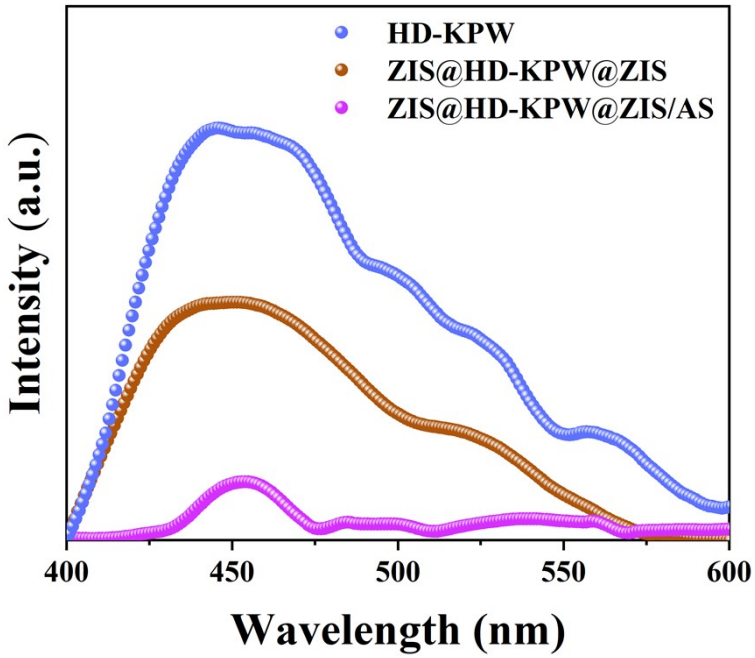

Fig. S23. Steady-state PL spectra of HD-KPW, ZIS@HD-KPW@ZIS and ZIS@HD-KPW@ZIS/AS.

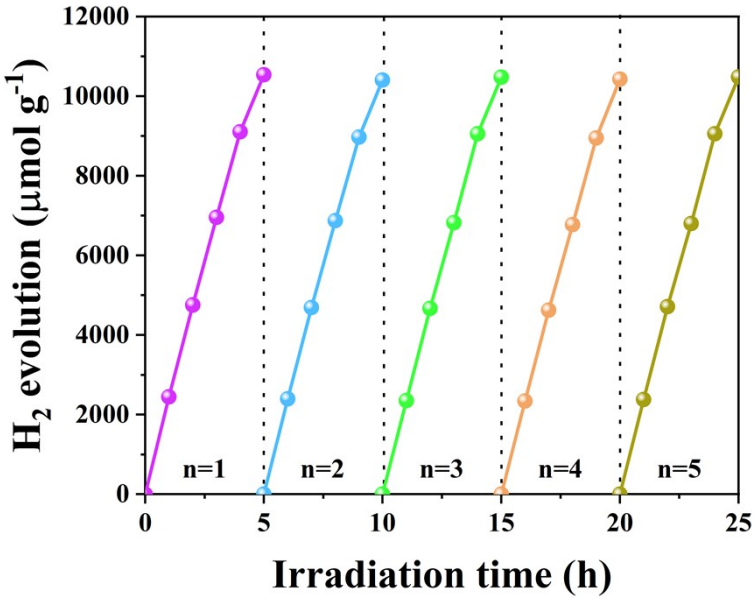

Fig. S24. Photocatalytic H_2 evolution cycle tests of ZIS@HD-KPW@ZIS/AS.

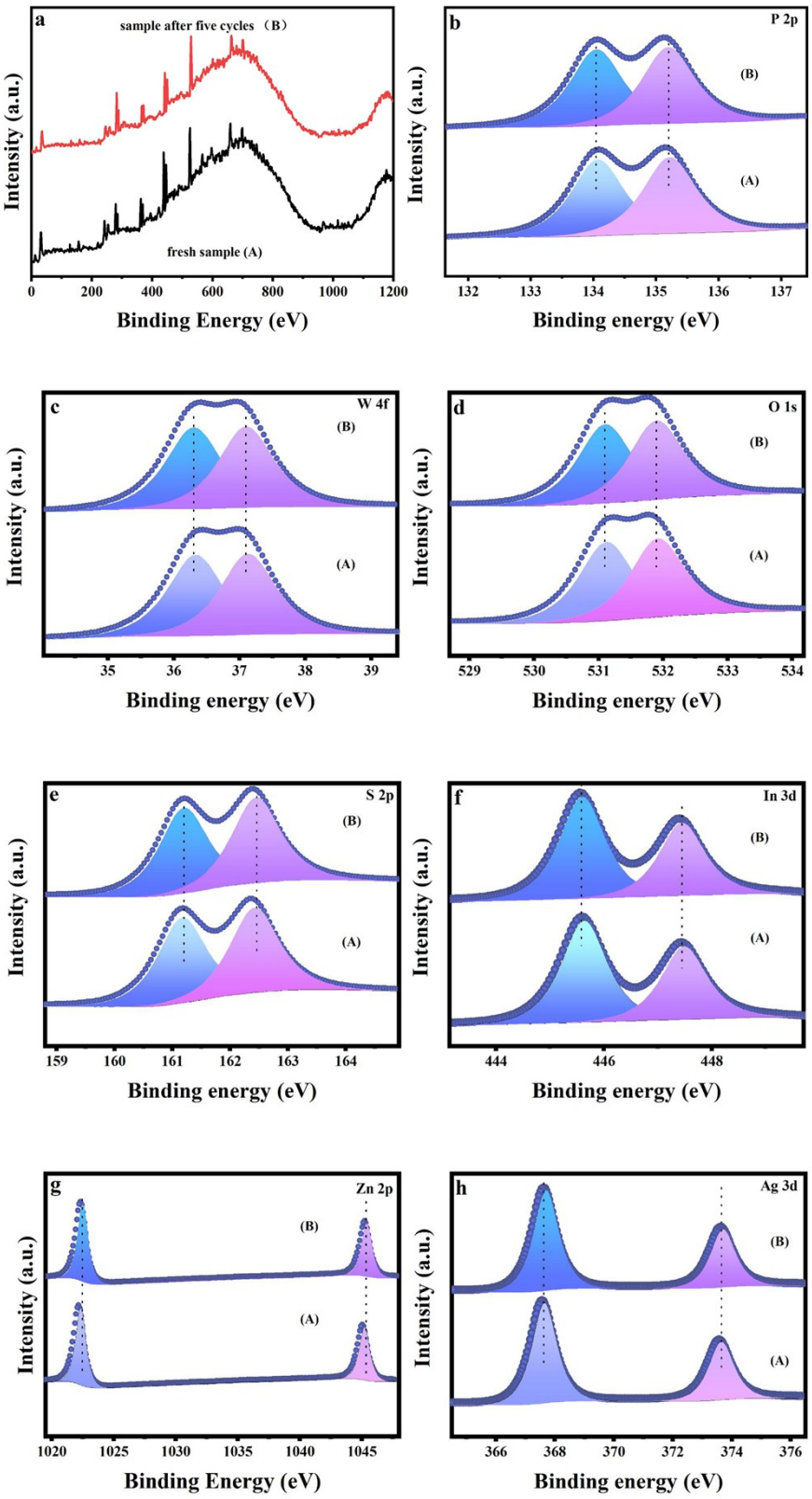

Fig. S25. The XPS spectra of ZIS@HD-KPW@ZIS/AS before (A) and after (B) five cycles of photocatalytic H_2 tests including survey (a), P 2p (b), W 4f (c), O 1s (d), S 2p (e), In 3d (f), Zn 2p (g) and Ag 3d (h).

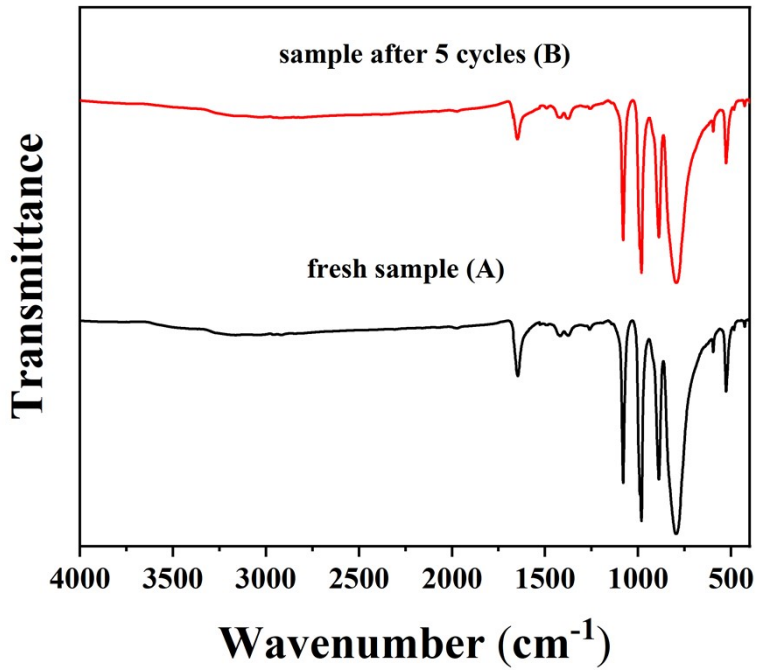

Fig. S26. The FT-IR spectra of ZIS@HD-KPW@ZIS/AS before (A) and after (B) five cycles of photocatalytic H_2 tests

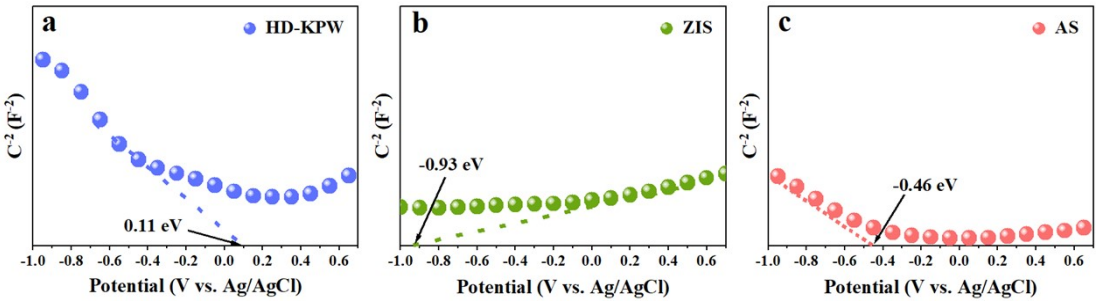

Fig. S27. Mott-Schottky curves of HD-KPW (a), ZIS (b) and AS (c), respectively.

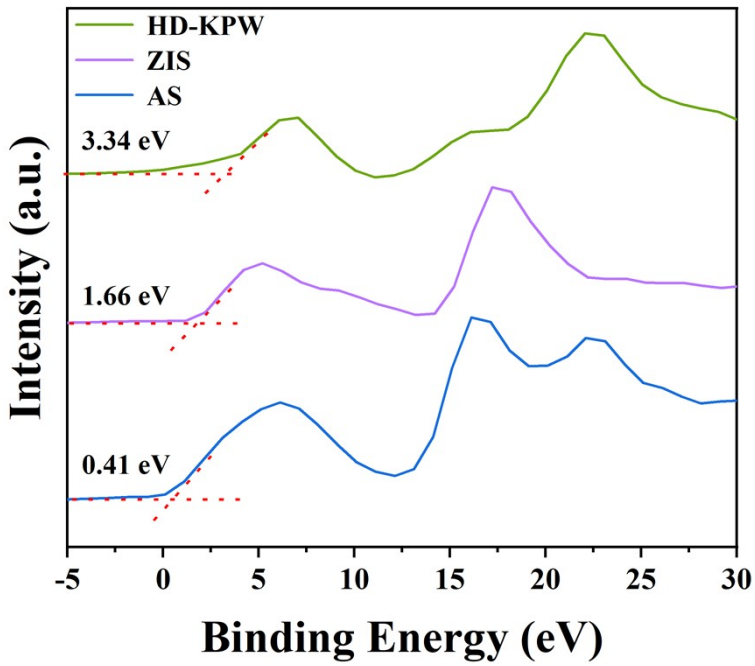

Fig. S28. VB of HD-KPW, ZIS and AS obtained by XPS.

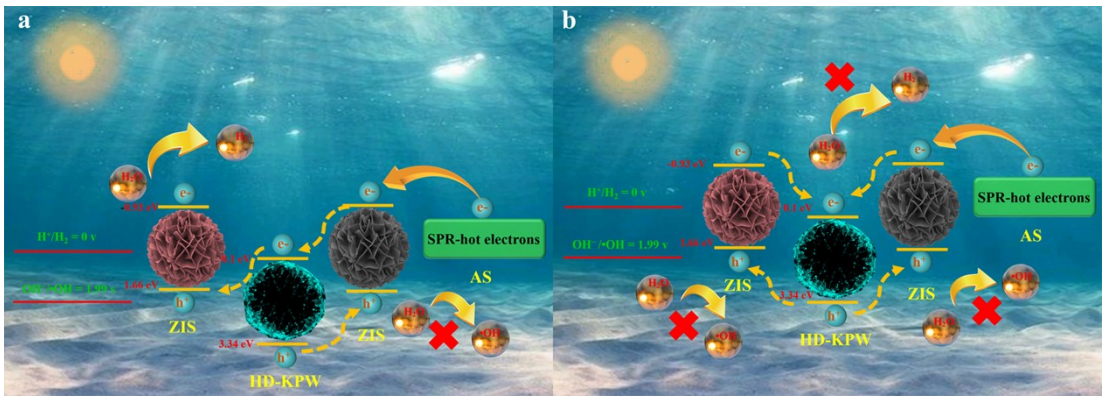

Fig. S29. Schematic diagrams of possible mechanisms of Z-scheme and type-II tandem heterojunctions (a) and dual type-II tandem heterojunctions (b).

Table S1. Comparison of tetracycline hydrochloride removal for different photocatalysts under light irradiation.

Photocatalysts	**Light source**	**Degradation rate**	**pollutant**	**Ref.**
CQD/$ZnIn_2S_4$	250 W Xe lamp (λ>420 nm)	85.07%	tetracycline hydrochloride	[1]
$WO_{2.72}$/$ZnIn_2S_4$	300 W Xe lamp (λ>400 nm)	97.3%	tetracycline hydrochloride	[2]
$ZnIn_2S_4$/MoO_3	300 W Xe lamp (λ>420 nm)	94.5%	tetracycline hydrochloride	[3]
Ag/Ag_2S/Bi_2MoO_6	300 W Xe lamp (λ>400 nm)	92.8%	tetracycline hydrochloride	[4]
$BiVO_4$/Ag@N-CQDs	300 W Xe lamp (λ>420 nm)	80.37%	tetracycline hydrochloride	[5]
This work	**300 W Xe lamp (λ>420 nm)**	**99%**	**tetracycline hydrochloride**	

Table S2. The specific BET surface areas and pore sizes of HD-KPW, ZIS@HD-KPW@ZIS and ZIS@HD-KPW@ZIS/AS.

Sample	S_{BET} ($m^2 g^{-1}$)	Pore size (nm)
HD-KPW	12.1	9.97
ZIS@HD-KPW@ZIS	24.1	10.45
ZIS@HD-KPW@ZIS/AS	27.4	9.06

Table S3. Comparison of photocatalytic H_2 evolution performance for $ZnIn_2S_4$-based photocatalysts.

Photocatalysts	**Light source**	**H_2 evolution rate ($\mu mol\ h^{-1}\ g^{-1}$)**	**References**
$rGO/TiO_2/ZnIn_2S_4$	300 W Xe lamp ($\lambda \geq 420$ nm)	462	[6]
$Ag_{0.2}Au_{0.8}/ZnIn_2S_4/TiO_2$	300 W Xe lamp ($\lambda > 420$ nm)	986	[7]
$ZnIn_2S_4$	300 W Xe lamp ($\lambda > 420$ nm)	1582	[8]
$SiO_2@TiO_2@ZnIn_2S_4$	300 W Xe lamp ($\lambda > 420$ nm)	618	[9]
$UiO\text{-}66@ZnIn_2S_4$	300 W Xe lamp ($\lambda > 420$ nm)	1860	[10]
ZIS@HD-KPW@ZIS/AS	**300W Xenon lamp, ≥420 nm**	**2107**	**This work**

Table 4. Band gap energies and potential positions of VB and CB of the used semiconductors of the composite.

Catalyst	E_g (eV)	E_{VB} (eV)	E_{CB} (eV)
HD-KPW	3.24	3.34	0.1
ZIS	2.59	1.66	-0.93
AS	0.87	0.41	-0.46

References

[1] H. Xu, Y. Jiang, X. Yang, F. Li, A. Li, Y. Liu, J. Zhang, Z. Zhou and L. Ni, *Mater. Res. Bull.,* 2018, **97**, 158.

[2] W. Chen, L. Chang, S. B. Ren, Z. C. He, G. B. Huang and X. H. Liu, *J. Hazard. Mater.,* 2020, **384**, 121308.

[3] C. Ouyang, X. Y. Quan, C. L. Zhang, Y. X. Pan, X. Y. Li, Z. L. Hong and M. J. Zhi, *Chem. Eng. J.,* 2021, **424**, 130510.

[4] S. J. Li, C. C Wang, Y. P Liu, B. Xue, W. Jiang, Y. Liu, L. Y. Mo and X. B. Chen, *Chem. Eng. J.,* 2021, **415**, 128991.

[5] J. Zhang, M. Y. Si, L. B. Jiang, X. Z. Yuan, H. B. Yu, Z. B. Wu, Y. F. Li and J. Y. Guo, *Chem. Eng. J.,* 2021, **410**, 128336.

[6] H. An, M. Li, W. Wang, Z. Lv, C. Deng, J. Huang and Z. Yin, *Ceram. Int.,* 2019, **45**, 14976.

[7] H. An, H. Wang, J. Huang, M. Li, W. Wang and Z. Yin, *Appl. Surf. Sci.,* 2019, **484**, 1168.

[8] C. Liao, J. Li, Y. Zhang, Y. Qu, P. Jiang, R. Cong and T. Yang, *Mater. Lett.,* 2019, **248**, 52.

[9] L. Wang, H. Zhou, H. Zhang, Y. Song, H. Zhang and X. Qian, *Inorg. Chem.,* 2020, **59**, 2278.

[10] J. F. Jiang, Q. Zhu, Y. Guo, L. Cheng, Y. B. Lou and J. X. Chen, *Chem. Soc. Jpn.,* 2019, **92**, 1047.